Journal of Computational Physics **172,** 235–260 (2001)
doi:10.1006/jcph.2001.6822, available online at http://www.idealibrary.com on IDEAL®

A Unified Coordinate System for Solving the Three-Dimensional Euler Equations

W. H. Hui and S. Kudriakov

Department of Mathematics and Center for Scientific Computation, The Hong Kong University of Science and Technology, Clear Water Bay, Hong Kong
E-mail: whhui@ust.hk

Received July 26, 2000; revised January 12, 2001

Two general coordinate systems have been used extensively in computational fluid dynamics: the Eulerian and the Lagrangian. The Eulerian coordinates cause excessive numerical diffusion across flow discontinuities, slip lines in particular. The Lagrangian coordinates, on the other hand, can resolve slip lines sharply but cause severe grid deformation, resulting in large errors and even breakdown of the computation. Recently, Hui *et al.* (*J. Comput. Phys.* **153**, 596 (1999)) have introduced a unified coordinate system which moves with velocity $h\mathbf{q}$, $\mathbf{q}$ being velocity of the fluid particle. It includes the Eulerian system as a special case when $h = 0$ and the Lagrangian when $h = 1$ and was shown to be superior to both Eulerian and Lagrangian systems for the two-dimensional Euler equations of gas dynamics when h is chosen to preserve the grid angles. The main purpose of this paper is to extend the work of Hui *et al.* to the three-dimensional Euler equations. In this case, the free function h is chosen so as to preserve grid skewness. This results in a coordinate system which avoids the excessive numerical diffusion across slip lines in the Eulerian coordinates and avoids severe grid deformation in the Lagrangian coordinates; yet it retains sharp resolution of slip lines, especially for steady flow.

Key Words: unified description; Eulerian description; Lagrangian description; inviscid compressible flow; slip lines; hyperbolicity of Euler equations.

1. INTRODUCTION

It is well known that the use of Eulerian coordinates for shock capturing methods results in badly smeared slip lines, and that Lagrangian coordinates, while capable of producing sharp slip line resolution, may result in severe grid deformation, causing inaccuracy and even breakdown of computation. A unified coordinate system was recently introduced (by Hui *et al.* [1]) in which the flow variables are considered to be functions of time and of some permanent identification of *pseudo-particles* which move with velocity $h\mathbf{q}$, $\mathbf{q}$ being the

0021-9991/01 $35.00

velocity of fluid particles. It includes the Eulerian coordinates as special case when $h = 0$ and the Lagrangian when $h = 1$. For two-dimensional inviscid flow as governed by the Euler equations of gas dynamics, the free function h is chosen so as to preserve grid angles. This results in a coordinate system which avoids excessive numerical diffusion across slip lines in the Eulerian coordinates and avoids severe grid deformations in the Lagrangian coordinates; yet it retains sharp resolution of slip lines, especially for steady flow.

The purpose of this paper is to extend the work of [1] to the three-dimensional (3-D) Euler equations. Since a computational cell in the 3-D case has two grid angles, it is generally impossible for one free function in the unified coordinates, h, to be chosen to preserve both grid angles. Instead, we require that the free function h be chosen so that the skewness of computational cells be preserved during the time marching. This has proved to be successful in that the unified coordinate system yields results which are superior to the Eulerian system in slip (contact) line resolution and which avoids severe grid deformation in the Lagrangian system.

In Section 2, the 3-D Euler equations are written in the unified coordinates. Section 3 explains how the free function h is to be determined to preserve grid skewness. Section 4 outlines the Riemann solution to the 1-D problem resulting from splitting of the 3-D Euler equations. This Riemann solution is then used in Section 5 to build an algorithm. Section 6 gives solutions to two test problems showing the advantages of the unified coordinates and, finally, concluding remarks are given in Section 7.

2. 3-D EULER EQUATIONS WRITTEN IN THE UNIFIED COORDINATES

2.1. *The Euler Equations of Gas Dynamics*

The 3-D unsteady inviscid polytropic gas flow is governed, under Eulerian description, by the conservation laws

$$\frac{\partial \mathbf{E}}{\partial t} + \frac{\partial \mathbf{F}}{\partial x} + \frac{\partial \mathbf{G}}{\partial y} + \frac{\partial \mathbf{H}}{\partial z} = \mathbf{0} \tag{1}$$

with

$$\mathbf{E} = \begin{bmatrix} \rho \\ \rho u \\ \rho v \\ \rho w \\ \rho e \end{bmatrix}, \quad \mathbf{F} = \begin{bmatrix} \rho u \\ \rho u^2 + p \\ \rho uv \\ \rho uw \\ \rho u\left(e + \frac{p}{\rho}\right) \end{bmatrix}, \quad \mathbf{G} = \begin{bmatrix} \rho v \\ \rho uv \\ \rho v^2 + p \\ \rho vw \\ \rho v\left(e + \frac{p}{\rho}\right) \end{bmatrix}, \quad \mathbf{H} = \begin{bmatrix} \rho w \\ \rho uw \\ \rho vw \\ \rho w^2 + p \\ \rho w\left(e + \frac{p}{\rho}\right) \end{bmatrix},$$

where t is the time variable, (x, y, z) are the Cartesian coordinates, and $\mathbf{q} = (u, v, w)^T$ is the flow velocity, with u, v, and w being the components in the x, y, and z directions, respectively. p and ρ are the pressure and density of the flow, respectively. The specific total energy e is

$$e = \frac{1}{2}q^2 + \frac{p}{(\gamma - 1)\rho}, \tag{2}$$

where γ is the ratio of specific heats of the gas, assumed constant, and $q = \sqrt{u^2 + v^2 + w^2}$ is the flow speed.

Under the transformation of variables [1]

$$\begin{cases} dt = d\lambda \\ dx = hud\lambda + Ad\xi + Ld\eta + Pd\zeta \\ dy = hud\lambda + Bd\xi + Md\eta + Qd\zeta \\ dz = hwd\lambda + Cd\xi + Nd\eta + Rd\zeta \end{cases} \tag{3}$$

the Euler equations (1) become

$$\frac{\partial \mathbf{E}}{\partial \lambda} + \frac{\partial \mathbf{F}}{\partial \xi} + \frac{\partial \mathbf{G}}{\partial \eta} + \frac{\partial \mathbf{H}}{\partial \zeta} = 0, \tag{4}$$

where

$$\mathbf{E} = \begin{bmatrix} \rho\triangle \\ \rho\triangle u \\ \rho\triangle v \\ \rho\triangle w \\ \rho\triangle e \\ A \\ B \\ C \\ L \\ M \\ N \\ P \\ Q \\ R \end{bmatrix}, \quad \mathbf{F} = \begin{bmatrix} \rho I \\ \rho Iu + p\xi_x\triangle \\ \rho Iv + p\xi_y\triangle \\ \rho Iw + p\xi_z\triangle \\ \rho I\left(e + \frac{p}{\rho}\right) - p\xi_t\triangle \\ -hu \\ -hv \\ -hw \\ 0 \\ 0 \\ 0 \\ 0 \\ 0 \\ 0 \end{bmatrix},$$

$$\mathbf{G} = \begin{bmatrix} \rho J \\ \rho Ju + p\eta_x\triangle \\ \rho Jv + p\eta_y\triangle \\ \rho Jw + p\eta_z\triangle \\ \rho J\left(e + \frac{p}{\rho}\right) - p\eta_t\triangle \\ 0 \\ 0 \\ 0 \\ -hu \\ -hv \\ -hw \\ 0 \\ 0 \\ 0 \end{bmatrix}, \quad \mathbf{H} = \begin{bmatrix} \rho K \\ \rho Ku + p\zeta_x\triangle \\ \rho Kv + p\zeta_y\triangle \\ \rho Kw + p\zeta_z\triangle \\ \rho K\left(e + \frac{p}{\rho}\right) - p\zeta_t\triangle \\ 0 \\ 0 \\ 0 \\ 0 \\ 0 \\ 0 \\ -hu \\ -hv \\ -hw \end{bmatrix}$$

with

$$\triangle = \det \begin{pmatrix} A & L & P \\ B & M & Q \\ C & N & R \end{pmatrix} \tag{5}$$

$$I = \triangle(\xi_t + u\xi_x + v\xi_y + w\xi_z) = \triangle \frac{D\xi}{Dt} \tag{6}$$

$$J = \triangle(\eta_t + u\eta_x + v\eta_y + w\eta_z) = \triangle \frac{D\eta}{Dt} \tag{7}$$

$$K = \triangle(\zeta_t + u\zeta_x + v\zeta_y + w\zeta_z) = \triangle \frac{D\zeta}{Dt} \tag{8}$$

and

$$\frac{\partial(\lambda, \xi, \eta, \zeta)}{\partial(t, x, y, z)} = \left(\frac{\partial(t, x, y, z)}{\partial(\lambda, \xi, \eta, \zeta)} \right)^{-1}. \tag{9}$$

We note that the first five equations of (4) express the physical laws of conservation of mass, momentum, and energy, whereas the last nine equations of (4) are the compatibility conditions for dx, dy, and dz in the transformation (3) to be total differentials. They are also called *geometric conservation laws*.

The most important properties of the unified coordinates are the following:

(a) The coordinates (ξ, η, ζ) are material functions of the pseudo-particles whose velocities are $h\mathbf{q}$. Indeed,

$$\frac{D_h\xi}{Dt} = 0, \quad \frac{D_h\eta}{Dt} = 0, \quad \frac{D_h\zeta}{Dt} = 0, \tag{10}$$

where

$$\frac{D_h}{Dt} \equiv \frac{\partial}{\partial t} + hu\frac{\partial}{\partial x} + hv\frac{\partial}{\partial y} + hw\frac{\partial}{\partial z} \tag{11}$$

is the material derivative following a pseudo-particle. Consequently, computational cells move and deform with the pseudo-particles rather than the fluid particles.

(b) In the special case when $h = 0$, $(A, L, \ldots, R)$ are independent of λ. Then the coordinates (ξ, η, ζ) are independent of time λ and are hence fixed in space; this coordinate system is thus Eulerian.

In the special case when $h = 1$, on the other hand, the pseudo-particles coincide with fluid particles and (ξ, η, ζ) are the material functions of fluid particles, and hence are Lagrangian coordinates.

In the general case, h is arbitrary. It thus provides a new degree of freedom which may be used to advantage: to avoid severe grid deformation in Lagrangian coordinates. It will be shown in this paper that this can be achieved for 3-D flow if h is chosen to preserve grid skewness.

(c) In steady flow, pathlines are identical with streamlines. Hence a slip line, which is necessarily a pathline, coincides with the streamline of a fluid particle and, therefore, also with the streamline of a pseudo-particle. Consequently, it can be taken to correspond to one of the coordinates, ξ^* say, thus avoiding the Godunov averaging across it. Therefore, *in the*

unified coordinate system a slip line can be sharply resolved. This is in direct contrast to the Eulerian coordinate system where a slip line does not coincide with a coordinate line and, as a result, the Godunov averaging across a slip line in a computational cell will forever smear it.

2.2. *Hyperbolicity*

It is shown in [2] that the three-dimensional system of unsteady Euler equations in the unified coordinates remains hyperbolic except in the case $h \equiv 1$ (Lagrangian). In the latter case it is weakly hyperbolic, meaning that while all eigenvalues are real, there does not exist a complete set of linearly independent eigenvectors. To avoid possible difficulties, such as the existence and uniqueness of weak solutions, arising from the lack of a complete set of eigenvectors, we shall use $h = 0.999$ (or any h very close to 1.0), for which the Euler equations are hyperbolic, and shall loosely refer it to be Lagrangian (see Section 5.1 for further comments).

2.3. *Solution Strategies*

As the system of Euler equations (4) written in unified coordinates is in conservation form, any well-established shock-capturing method can be used to solve it. We shall use the unsplit finite volume method applying the Godunov upwind fluxes across each intercell boundary with the MUSCL update to higher resolution in space to solve system (4). The computation will be done entirely in the λ–ξ–η–ζ space. A physical cell in the x–y–z plane marching along the pseudo-particle's pathline corresponds to a rectangular cell in the ξ–η–ζ plane marching in the λ direction in the computational space λ–ξ–η–ζ. The superscript n refers to the marching time step number and the subscripts i, j, and k refer to the cell index number on a time plane $\lambda = \text{const}$. The time step $\Delta\lambda^n = \lambda^{n+1} - \lambda^n$ is uniform for all i, j, and k, but is always chosen to satisfy the CFL stability condition. The grid divides the computational domain into cubic control volumes, or cells, which in the ξ, η, and ζ directions are centered at $(\lambda^n, \xi_i, \eta_j, \zeta_k)$ and have widths $\Delta\xi_i = \xi_{i+1/2} - \xi_{i-1/2}$, $\Delta\eta_j = \eta_{j+1/2} - \eta_{j-1/2}$ and $\Delta\zeta_k = \zeta_{k+1/2} - \zeta_{k-1/2}$ (for all n). Unless otherwise stated we shall use uniform cell width $\Delta\xi_i$ for all i, $\Delta\eta_j$ for all j and $\Delta\zeta_k$ for all k.

In the physical space (t, x, y, z) a cuboid cell marching in $(\lambda, \xi, \eta, \zeta)$ space corresponds to a pseudo-particle moving along its path tube with step Δt ($\Delta t = \Delta\lambda$). The pseudo-particle is bounded by six path surfaces $\xi = \xi_{i\pm1/2}$, $\eta = \eta_{j\pm1/2}$ and $\zeta = \zeta_{k\pm1/2}$ around its center. Initially, any curvilinear coordinate grid in the x–y–z space may be used as the ξ–η–ζ coordinate grid and the initial geometric variables $\mathbf{K} = (A, B, C, L, M, N, P, Q, R)^T$ determined from (3) as part of the initial conditions. A stationary solid wall is always a path surface of the fluid and hence also of the pseudo-fluid [1]; it is therefore a coordinate surface of the unified coordinates.

Applying the divergence theorem to (4) over the cuboid cell (i, j, k, n) results in

$$\mathbf{E}^{n+1}_{i,j,k} = \mathbf{E}^{n}_{i,j,k} - \frac{\Delta\lambda^n}{\Delta\xi_i}\left(\mathbf{F}^{n+1/2}_{i+1/2,j,k} - \mathbf{F}^{n+1/2}_{i-1/2,j,k}\right) - \frac{\Delta\lambda^n}{\Delta\eta_j}\left(\mathbf{G}^{n+1/2}_{i,j+1/2,k} - \mathbf{G}^{n+1/2}_{i,j-1/2,k}\right) - \frac{\Delta\lambda^n}{\Delta\zeta_k}\left(\mathbf{H}^{n+1/2}_{i,j,k+1/2} - \mathbf{H}^{n+1/2}_{i,j,k-1/2}\right) \tag{12}$$

with $i = 1, 2, \ldots, i_{max}$; $j = 1, 2, \ldots, j_{max}$; $k = 1, 2, \ldots, k_{max}$, where the notations for the cell-averages of any quantity f are

$$f^n_{i,j,k} = \frac{1}{\Delta\xi_i \Delta\eta_j \Delta\zeta_k} \int_{\xi_{i-1/2}}^{\xi_{i+1/2}} \int_{\eta_{j-1/2}}^{\eta_{j+1/2}} \int_{\zeta_{k-1/2}}^{\zeta_{k+1/2}} f(\lambda^n, \xi, \eta, \zeta)\, d\xi\, d\eta\, d\zeta, \tag{13}$$

and

$$f^{n+1/2}_{i+1/2,j,k} = \frac{1}{\Delta\lambda^n \Delta\eta_j \Delta\zeta_k} \int_{\lambda^n}^{\lambda^{n+1}} \int_{\eta_{j-1/2}}^{\eta_{j+1/2}} \int_{\zeta_{k-1/2}}^{\zeta_{k+1/2}} f\left(\lambda, \xi_{i+1/2}, \eta, \zeta\right) d\lambda\, d\eta\, d\zeta, \tag{14}$$

$$f^{n+1/2}_{i,j+1/2,k} = \frac{1}{\Delta\lambda^n \Delta\xi_i \Delta\zeta_k} \int_{\lambda^n}^{\lambda^{n+1}} \int_{\xi_{i-1/2}}^{\xi_{i+1/2}} \int_{\zeta_{k-1/2}}^{\zeta_{k+1/2}} f\left(\lambda, \xi, \eta_{j+1/2}, \zeta\right) d\lambda\, d\xi\, d\zeta, \tag{15}$$

$$f^{n+1/2}_{i,j,k+1/2} = \frac{1}{\Delta\lambda^n \Delta\xi_i \Delta\eta_j} \int_{\lambda^n}^{\lambda^{n+1}} \int_{\xi_{i-1/2}}^{\xi_{i+1/2}} \int_{\eta_{j-1/2}}^{\eta_{j+1/2}} f\left(\lambda, \xi, \eta, \zeta_{k+1/2}\right) d\lambda\, d\xi\, d\eta. \tag{16}$$

According to Godunov's idea used in our paper, the cell-interface fluxes $\mathbf{F}^{n+1/2}_{i+1/2,j,k}$, $\mathbf{G}^{n+1/2}_{i,j+1/2,k,}$ and $\mathbf{H}^{n+1/2}_{i,j,k+1/2}$ for the cell (i, j, k) are to be obtained from the self-similar solution of local one-dimensional Riemann problems formed by the averaged constant state $\mathbf{E}_{i,j,k}$ of the cell (i, j, k) and those of its adjacent cells.

We remark that the above solution strategies place no restriction on the free function h.

3. DETERMINATION OF h

The chief advantage of the unified coordinates is the new degree of freedom in choosing h. The simplest way would be to choose a constant value for h: choosing $h = 0$ leads to Eulerian formulation which is highly diffusive, especially in the resolution of contact surfaces; on the other hand, choosing $h = 0.999$ (effectively Lagrangian formulation) gives excellent resolution of contact surfaces, but the computation may fail due to severe grid deformation. A choice of constant h between 0.0 and 1.0 would yield results somewhere in between the Eulerian and the Lagrangian.

The main question is: what condition should be imposed on h in order to reduce numerical diffusion near discontinuities while avoiding severe grid deformation.

For two-dimensional flow, as shown in [1], a good choice for h is to preserve the grid angles in the solution process which marches in λ. Unfortunately, this idea cannot be implemented for three-dimensional flow because there is now more than one grid angle for each cell, and one free function h cannot, in general, be chosen to preserve more than one angle.

To see this, we note from the transformation (3) that, with $\mathbf{r} = (x, y, z)^T$,

$$\frac{\partial \mathbf{r}}{\partial \xi} = (A, B, C)^T \equiv \mathbf{A} \tag{17}$$

$$\frac{\partial \mathbf{r}}{\partial \eta} = (L, M, N)^T \equiv \mathbf{L} \tag{18}$$

$$\frac{\partial \mathbf{r}}{\partial \zeta} = (P, Q, R)^T \equiv \mathbf{P}. \tag{19}$$

For 2-D flow, there is only one grid angle α for a cell

$$\alpha = \cos^{-1} \frac{\mathbf{A} \cdot \mathbf{L}}{|\mathbf{A}||\mathbf{L}|}, \tag{20}$$

whereas there exists another grid angle β

$$\beta = \sin^{-1} \left(\frac{\mathbf{A} \times \mathbf{L}}{|\mathbf{A} \times \mathbf{L}|} \cdot \frac{\mathbf{P}}{|\mathbf{P}|} \right) \tag{21}$$

for a cell in 3-D flow. The special case of orthogonal grid corresponds to $\alpha = \beta = \frac{\pi}{2}$.

For 2-D flow, h can be chosen to preserve α, i.e.,

$$\frac{\partial \alpha}{\partial \lambda} = 0. \tag{22}$$

Since for 3-D flow, one free function h cannot be chosen to simultaneously preserve both angles α and β, we choose to preserve the grid skewness κ, i.e.,

$$\frac{\partial \kappa}{\partial \lambda} = 0, \tag{23}$$

where

$$\kappa \equiv \frac{|\mathbf{A}||\mathbf{L}||\mathbf{P}|}{(\mathbf{A} \times \mathbf{L}) \cdot \mathbf{P}} - 1 = \frac{1}{\sin\alpha \sin\beta} - 1. \tag{24}$$

From the definition of grid skewness κ, it is clear that

(a) κ is always non-negative;

(b) An orthogonal grid, i.e., $\alpha = \beta = \frac{\pi}{2}$, corresponds to $\kappa = 0$;

(c) A degenerated (or singular) grid, i.e., $\alpha = 0$ or $\beta = 0$ or both, corresponds to $\kappa = \infty$. In this case the Jacobian $\triangle = \det(\mathbf{A}, \mathbf{L}, \mathbf{P}) = (\mathbf{A} \times \mathbf{L}) \cdot \mathbf{P}$ of the transformation (3) is also singular; i.e., $\triangle = 0$;

(d) When grid skewness, κ, is preserved the Jacobian and hence the transformation (3) will not become singular during marching in λ. This, therefore, will prevent breakdown of computation and may also avoid severe grid deformation as happens in Lagrangian coordinates.

Now, skewness-preserving condition (23) is equivalent to

$$\frac{\partial (\kappa + 1)^2}{\partial \lambda} = \frac{\partial}{\partial \lambda} \left(\frac{|\mathbf{A}||\mathbf{L}||\mathbf{P}|}{\triangle} \right)^2 = 0 \tag{25}$$

which, upon using the last nine equations of (4), leads to an equation for h as follows

$$a \frac{\partial h}{\partial \xi} + b \frac{\partial h}{\partial \eta} + c \frac{\partial h}{\partial \zeta} + d \cdot h = 0, \tag{26}$$

where

$$a = \mathbf{q} \cdot \left(\frac{\mathbf{A}}{|\mathbf{A}|^2} - \nabla \xi \right) \tag{27}$$

$$b = \mathbf{q} \cdot \left(\frac{\mathbf{L}}{|\mathbf{L}|^2} - \nabla \eta \right) \tag{28}$$

$$c = \mathbf{q} \cdot \left(\frac{\mathbf{P}}{|\mathbf{P}|^2} - \nabla \zeta \right) \tag{29}$$

$$d = \frac{\partial \mathbf{q}}{\partial \xi} \cdot \left(\frac{\mathbf{A}}{|\mathbf{A}|^2} - \nabla \xi \right) + \frac{\partial \mathbf{q}}{\partial \eta} \cdot \left(\frac{\mathbf{L}}{|\mathbf{L}|^2} - \nabla \eta \right) + \frac{\partial \mathbf{q}}{\partial \zeta} \cdot \left(\frac{\mathbf{P}}{|\mathbf{P}|^2} - \nabla \zeta \right). \tag{30}$$

Equation (26) is a first-order partial differential equation for $h(\xi, \eta, \zeta; \lambda)$, with λ appearing as a parameter. To find solution h in the range

$$0 \le h \le 1 \tag{31}$$

we note that (26) is linear and homogeneous and, as such, possesses two properties:

(a) positive solution $h > 0$ always exists;
(b) if h is a solution to (26) so is h/C, C being any constant.

Making use of property (a), we let $g = \ln(hq)$ to get

$$a \frac{\partial g}{\partial \xi} + b \frac{\partial g}{\partial \eta} + c \frac{\partial g}{\partial \zeta} + d_1 = 0, \tag{32}$$

where

$$d_1 = q \left(\frac{\partial \mathbf{q}/q}{\partial \xi} \cdot \left[\frac{\mathbf{A}}{|\mathbf{A}|^2} - \nabla \xi \right] \right) + q \left(\frac{\partial \mathbf{q}/q}{\partial \eta} \cdot \left[\frac{\mathbf{L}}{|\mathbf{L}|^2} - \nabla \eta \right] \right) + q \left(\frac{\partial \mathbf{q}/q}{\partial \zeta} \cdot \left[\frac{\mathbf{P}}{|\mathbf{P}|^2} - \nabla \zeta \right] \right). \tag{33}$$

Now, if g_1 is any solution to (32) then $h = e^{g_1}/qC$ is a solution to (26) satisfying condition (31), provided we choose C equal to the maximum of e^{g_1}/q over the whole flow field being computed. The reason to work with $\ln(hq)$ instead of $\ln(h)$ is that from our experience with steady supersonic flow [3], hq is continuous across slip lines; hence working with hq can minimize the numerical errors.

Numerically, Eq. (32) is solved by iteration for non-orthogonal grids.

In the special case of the orthogonal grid, it can be shown that

$$\frac{\mathbf{A}}{|\mathbf{A}|^2} - \nabla \xi = \frac{\mathbf{L}}{|\mathbf{L}|^2} - \nabla \eta = \frac{\mathbf{P}}{|\mathbf{P}|^2} - \nabla \zeta = 0. \tag{34}$$

To see this, we first note that

$$\nabla \xi \cdot \mathbf{A} = 1, \quad \nabla \xi \cdot \mathbf{L} = 0, \quad \nabla \xi \cdot \mathbf{P} = 0 \tag{35}$$

meaning that $\nabla \xi \perp \mathbf{L}$ and $\nabla \xi \perp \mathbf{P}$. If the coordinates are orthogonal, i.e.,

$$\mathbf{A} \perp \mathbf{L}, \quad \mathbf{A} \perp \mathbf{P}, \tag{36}$$

then from (35) and (36) follows

$$\frac{\mathbf{A}}{|\mathbf{A}|} = \frac{\nabla\xi}{|\nabla\xi|}, \tag{37}$$

which after substitution into the first equation of (35) leads to

$$|\nabla\xi| = \frac{1}{|\mathbf{A}|}. \tag{38}$$

Finally, using (37) and (38) we get

$$\nabla\xi = |\nabla\xi|\frac{\nabla\xi}{|\nabla\xi|} = |\nabla\xi|\frac{\mathbf{A}}{|\mathbf{A}|} = \frac{\mathbf{A}}{|\mathbf{A}|^2}. \tag{39}$$

Similarly,

$$\nabla\eta = \frac{\mathbf{L}}{|\mathbf{L}|^2} \tag{40}$$

$$\nabla\zeta = \frac{\mathbf{P}}{|\mathbf{P}|^2}. \tag{41}$$

Hence

$$a = b = c = d = 0 \tag{42}$$

and Eq. (26) becomes singular; consequently h is left undetermined, while there is no guarantee that the grid skewness—orthogonality in this case—is preserved. (If this were not the case, then an h can be chosen to preserve grid orthogonality in 3-D flow, in particular 3-D steady supersonic flow; this would then contradict the finding of [4] that orthogonal grid for steady supersonic flow with streamlines coinciding with coordinate lines does not exist unless the flow is complex-lamellar, meaning $\mathbf{q}\cdot\nabla\times\mathbf{q}\equiv 0$). Numerically this difficulty can be avoided: if the grid is orthogonal we do not solve Eq. (26) to get h; rather, we take $h = 0.999$, allowing the grid to deform with the flow until $(|a| + |b| + |c| + |d|) > \epsilon$. For our computations we found it satisfactory to take $\epsilon = 10^{-4}$. Once the grid is deformed it is no longer orthogonal and the skewness will be preserved in time according to (26), which is now regular.

In the special case of two-dimensional flow, $\beta = \frac{\pi}{2}$; hence $\kappa = \frac{1}{\sin\alpha} - 1$ and condition (23) reduces to

$$\cos\alpha\frac{\partial\alpha}{\partial\lambda} = 0, \tag{43}$$

which is the same as (22) except for the important case of orthogonal grid for which $\alpha = \frac{\pi}{2}$, giving $\cos\alpha = 0$. In the latter case, therefore, imposing $\frac{\partial\kappa}{\partial\lambda} = 0$ does not necessarily lead to $\frac{\partial\alpha}{\partial\lambda} = 0$; i.e., it does not lead to determining the free function h. Therefore, for 2-D flow, it is better to use the grid angle preserving condition (22) than the grid skewness preserving condition (23) so as to cover the important case of the orthogonal grid.

Computationally, as in the 2-D case [1], Eq. (26) is to be solved at every time step after the flow variables $\mathbf{Q} = (p, \rho, u, v, w)^T$ and the geometric variables $\mathbf{K} = (A, B, C, L, M, N, P, Q, R)^T$ are updated.

In closing, we remark that alternative methods of determining h are possible. For instance, h can be chosen to preserve the Jacobian Δ of the transformation (3). But this in the 2-D case cannot preserve grid orthogonality which, of course, represents the case of optimal coordinates.

4. THE ξ-SPLIT RIEMANN PROBLEM

The ξ-split Riemann problem is obtained by assuming that $\frac{\partial}{\partial \eta} = 0$ and $\frac{\partial}{\partial \zeta} = 0$ in (4) and is given by

$$\begin{cases} \frac{\partial \mathbf{E}}{\partial \lambda} + \frac{\partial \mathbf{F}}{\partial \xi} = \mathbf{0} \quad \lambda > 0, \quad -\infty < \xi < +\infty \\ \mathbf{E}(0, \xi) = \begin{cases} \mathbf{E}_l, & \xi < 0 \\ \mathbf{E}_r, & \xi > 0, \end{cases} \end{cases} \tag{44}$$

where

$$\mathbf{E} = \begin{bmatrix} \rho\triangle \\ \rho\triangle u \\ \rho\triangle v \\ \rho\triangle w \\ \rho\triangle e \\ A \\ B \\ C \\ L \\ M \\ N \\ P \\ Q \\ R \end{bmatrix}, \quad \mathbf{F} = \begin{bmatrix} \rho\triangle(1-h)(\mathbf{q}\cdot\nabla\xi) \\ \rho\triangle(1-h)u(\mathbf{q}\cdot\nabla\xi) + p\triangle\xi_x \\ \rho\triangle(1-h)v(\mathbf{q}\cdot\nabla\xi) + p\triangle\xi_y \\ \rho\triangle(1-h)w(\mathbf{q}\cdot\nabla\xi) + p\triangle\xi_z \\ \rho\triangle(1-h)e(\mathbf{q}\cdot\nabla\xi) + p\triangle(\mathbf{q}\cdot\nabla\xi) \\ -hu \\ -hv \\ -hw \\ 0 \\ 0 \\ 0 \\ 0 \\ 0 \\ 0 \end{bmatrix},$$

with

$$\triangle = \det \begin{pmatrix} A & L & P \\ B & M & Q \\ C & N & R \end{pmatrix} \tag{45}$$

$$e = \frac{1}{2}(u^2 + v^2 + w^2) + \frac{p}{(\gamma - 1)\rho}. \tag{46}$$

The vectors $\mathbf{E}_l$ and $\mathbf{E}_r$ in (44) are constant.

Hereafter we shall abandon the last six equations of the system (44), keeping in mind that $\mathbf{L} = \mathbf{L}_{l,r}$ and $\mathbf{P} = \mathbf{P}_{l,r}$ are given constants.

In order to solve the Riemann problem (44) we project velocity vector $\mathbf{q}$ on the directions normal to the plane $\xi = \text{const.}$ and tangential to it. For that reason we introduce three orthogonal unit vectors $\mathbf{i}$, $\mathbf{j}$, $\mathbf{k}$, with $\mathbf{i}$ being normal to the coordinate plane $\xi = \text{const.}$ and $\mathbf{j}$ and $\mathbf{k}$ tangential to it. Accordingly,

$$\mathbf{i} \equiv (i_1, i_2, i_3) = \frac{1}{|\nabla \xi|}(\xi_x; \xi_y; \xi_z), \tag{47}$$

$$\mathbf{j} \equiv (j_1, j_2, j_3) = \begin{cases} \frac{1}{\sqrt{\xi_y^2 + \xi_z^2}}(0; -\xi_z; \xi_y) & \text{if } \xi_y^2 + \xi_z^2 \neq 0 \\ (0, 1, 0) & \text{if } \xi_y = \xi_z = 0, \end{cases} \tag{48}$$

$$\mathbf{k} \equiv (k_1, k_2, k_3) = \begin{cases} \frac{1}{|\nabla \xi|\sqrt{\xi_y^2 + \xi_z^2}}\left(\xi_y^2 + \xi_z^2; -\xi_x \xi_y; -\xi_x \xi_z\right) & \text{if } \xi_y^2 + \xi_z^2 \neq 0 \\ (0, 0, 1) & \text{if } \xi_y = \xi_z = 0 \end{cases}. \tag{49}$$

Let us rewrite (44) by using the component of velocity $\mathbf{q}$ in the direction $\mathbf{i}$ normal to, and $\mathbf{j}$ and $\mathbf{k}$ tangential to, the plane $\xi = \text{const.}$; i.e.,

$$\omega = \mathbf{q} \cdot \mathbf{i}, \quad \tau_1 = \mathbf{q} \cdot \mathbf{j}, \quad \tau_2 = \mathbf{q} \cdot \mathbf{k}. \tag{50}$$

The ξ-split Riemann problem (44) then becomes

$$\begin{cases} \frac{\partial \mathbf{E}}{\partial \lambda} + \frac{\partial \mathbf{F}}{\partial \xi} = \mathbf{0} \quad \lambda = 0, \quad -\infty < \xi < +\infty \\ \mathbf{E}(0, \xi) = \begin{cases} \mathbf{E}_l, & \xi < 0 \\ \mathbf{E}_r, & \xi > 0, \end{cases} \end{cases} \tag{51}$$

where

$$\mathbf{E} = \begin{bmatrix} \rho\triangle \\ \rho\triangle\omega \\ \rho\triangle\tau_1 \\ \rho\triangle\tau_2 \\ \rho\triangle e \\ A \\ B \\ C \end{bmatrix}, \quad \mathbf{F} = S \begin{bmatrix} \rho(1-h)\omega \\ \rho(1-h)\omega^2 + p \\ \rho(1-h)\omega\tau_1 \\ \rho(1-h)\omega\tau_2 \\ \rho(1-h)\omega e + \omega p \\ -hu/S \\ -hv/S \\ -hw/S \end{bmatrix},$$

with

$$S = \triangle \cdot |\nabla \xi| = \left(\begin{vmatrix} M & Q \\ N & R \end{vmatrix}^2 + \begin{vmatrix} L & P \\ N & R \end{vmatrix}^2 + \begin{vmatrix} L & P \\ M & Q \end{vmatrix}^2 \right)^{1/2}.$$

Our purpose is to find the flux $\mathbf{F}$ on $\zeta = 0$ to be used in the Godunov scheme to update the conserved quantities $\mathbf{E}$. Time level λ^n will be taken to be equal to 0 for convenience. h in

(51) is taken to be equal to $h_i^0 \equiv h_l$ for $\xi < 0$ and $h_{i+1}^0 \equiv h_r$ for $\xi > 0$. That is to say, they are assumed constant for $0 \le \lambda < \triangle\lambda$,

$$\frac{\partial h}{\partial \lambda} = 0 \quad (0 \le \lambda < \triangle\lambda) \tag{52}$$

and this is consistent with the equation for h (26). But h changes its value at $\lambda = \triangle\lambda$ as given by (26), whose coefficients are evaluated at $\lambda = \triangle\lambda$.

The detailes of obtaining the solution to the Riemann problem (51) are given in the Appendix.

5. NUMERICAL PROCEDURE

5.1. *Remarks on Our Numerical Method*

Before describing in detail the numerical procedure for solving the system (4) we make some remarks on our numerical method.

The first remark is related to the order of accuracy of the chosen method. Although Godunov–MUSCL scheme is used to give improved resolution in space, the accuracy in time in our computation is of first-order. In practice, however, the results for two-dimensional problems computed using our method are indistinguishable from the theoretically more accurate method obtained in [1] by using Strang splitting; Strang splitting in a three-dimensional case requires considerably more computing time.

Secondly, we emphasize the difference between the solution strategy used in [1] and that in the present paper. In [1] the split Riemann problems are solved using the time step-wise Eulerian approximation (TSE); namely, the Riemann problems for the physical conservation laws are solved while the geometric variables are kept unchanged. In the present work we do not need this additional approximation, because the split Riemann problems are solved for the geometric variables as well as for the physical variables (for example, in solving the ξ-split Riemann problem, the formulas for $\mathbf{A}$ can also be obtained although they are not needed in calculating the flux $\mathbf{F}$). In other words, TSE is not used in the present approach.

Lastly, in solving the split Riemann problems (see Appendix) we do not need to use explicitly the complete set of right eigenvectors. The eigenvectors that are used are those corresponding to the genuinely nonlinear characteristic families; these eigenvectors exist even in the case $h = 1$ (Lagrangian coordinates). The missing eigenvectors in Lagrangian coordinates correspond to the linearly degenerated characteristic families and are not employed in constructing solutions to the split Riemann problems. This also explains why our computations with $h = 1$ encounter no difficulty and produce results identical to that for $h = 0.999$ and also justifies calling the $h = 0.999$ solution a Lagrangian one. We have presented results for $h = 0.999$, rather than for $h = 1.0$, and called them Lagrangian because the theoretical base for the existence and uniqueness of the Riemann problem for $h = 1.0$ is not certain. We further note that if some approximate Riemann solver is used, for example, the Roe solver, or any other method which requires a complete set of eigenvectors, computation for the case $h = 1$ might have serious difficulties.

5.2. *Computational Steps*

Step 1 (Initialization). Assume the initial conditions of a flow problem are given at $t = 0$ ($\lambda = 0$) in the x–y–z space. Then an appropriate ξ–η–ζ coordinate grid is laid on the x–y–z plane (for instance, we take ξ, η, and ζ equal to the arc length of their corresponding coordinate line in the x–y–z space), with $\xi = \xi_0, \xi_1, \xi_2, \ldots, \xi_{i_{max}}$, $\eta = \eta_0, \eta_1, \eta_2, \ldots, \eta_{j_{max}}$, and $\zeta = \zeta_0, \zeta_1, \zeta_2, \ldots, \zeta_{k_{max}}$, the surface $\xi = \xi_0$ (or/and any other coordinate surface, depending on the problem) coinciding with the solid surface if there is one. Hence the conservative variables $\mathbf{E}^0_{i,j,k}$ are obtained by averaging the given flow over the computational cell (i, j, k). They are used together with $h^0_{i,j,k}$ as initial conditions. Subsequently, $\mathbf{Q}^0_{i,j,k} = (p^0, \rho^0, u^0, v^0, w^0)^T_{i,j,k}$, $i = 1, 2, \ldots, i_{max}$, $j = 1, 2, \ldots, j_{max}$, $k = 1, 2, \ldots, k_{max}$, are obtained from $\mathbf{E}^0_{i,j,k}$ by a decoding procedure described in Step 4. For example, if we choose ξ, η, ζ to be the respective arc lengths of x-, y-, and z-coordinate lines then, from (3), $\mathbf{K}^0_{i,j,k} = (1, 0, 0, 0, 1, 0, 0, 0, 1)^T$ and $\mathbf{Q}^0_{i,j,k}$ follow from the expressions for $\mathbf{E}^0_{i,j,k}$ in (4).

Step 2 (Construction of interface flux F). We first take

$$(\mathbf{L}_{i,j,k}(\lambda), \mathbf{P}_{i,j,k}(\lambda), h_{i,j,k}(\lambda)) = (\mathbf{L}_{i,j,k}(\lambda^n)\mathbf{P}_{i,j,k}(\lambda^n), h_{i,j,k}(\lambda^n)), \quad (\lambda^n \le \lambda < \lambda^{n+1}). \tag{53}$$

Then for every pair of adjacent cells (i, j, k) and $(i + 1, j, k)$,

(a) Define the normal direction of the cell interface $\xi_{i+\frac{1}{2},j,k}$ between the two adjacent cells (i, j, k) and $(i + 1, j, k)$ as

$$\mathbf{n} = \frac{(\nabla\xi)_{i,j,k} + (\nabla\xi)_{i+1,j,k}}{|(\nabla\xi)_{i,j,k} + (\nabla\xi)_{i+1,j,k}|}, \tag{54}$$

i.e., the average direction of $(\nabla\xi)_{i,j,k}$ and $(\nabla\xi)_{i+1,j,k}$. Expression (54) is an approximation to the expression for $\mathbf{n}$ in (47) for the cell interface $\xi_{i+\frac{1}{2},j,k}$. Project the velocity vector $\mathbf{q} = (u, v, w)$ into the normal and the tangential components (ω, τ_1, and τ_2) using Eq. (50).

(b) Do a MUSCL type data reconstruction in a component-by-component manner. For example, in the ξ direction, let f be any of the above physical variables p, ρ, $\omega\tau_1$, τ_2, then, instead of assuming a uniform state in the cells (i, j, k) and $(i + 1, j, k)$, we assume linearly distributed states and use linear extrapolation to determine cell interface flow variables: $f_r = f_{i+1,j,k} - 0.5(f_{i+2,j,k} - f_{i+1,j,k})\phi(r^+)$ with $r^+ = (f_{i+1,j,k} - f_{i,j,k})/(f_{i+2,j,k} - f_{i+1,j,k})$ and $f_\ell = f_{i,j,k} + 0.5(f_{i,j,k} - f_{i-1,j,k})\phi(r^-)$ with $r^- = (f_{i+1,j,k} - f_{i,j,k})/(f_{i,j,k} - f_{i-1,j,k})$, where $\phi(r) = \max(0, \min(1, r))$ is the minmod flux limiter and subscripts r and ℓ of f correspond to right and left states, respectively.

(c) Solve the Riemann problem of (51) as explained in the Appendix to get the interfacial flow variables $(p, \rho, \omega, \tau_1, \tau_2)^T$ and hence $(p, \rho, u, v, w)^T$ at the cell interface $\xi = \xi_{i+\frac{1}{2},j,k}$. These are constants and will be denoted by $(\cdot)^{n+1/2}_{i+\frac{1}{2},j,k}$. The flux $\mathbf{F}$ is then determined using values of $\mathbf{L}$ and $\mathbf{P}$ at n level and the Riemann solution for $\mathbf{Q}$ on cell interfaces.
The interfacial fluxes $\mathbf{G}$ and $\mathbf{H}$ can be constructed in a similar way.

Step 3 (Update the conserved variables E). The conservative variables $\mathbf{E}^{n+1}_{i,j,k}$ are updated as follows

$$\begin{aligned}\mathbf{E}^{n+1}_{i,j,k} = \mathbf{E}^n_{i,j,k} &- \frac{\Delta\lambda^n}{\Delta\xi_i}\left(\mathbf{F}^{n+1/2}_{i+1/2,j,k} - \mathbf{F}^{n+1/2}_{i-1/2,j,k}\right) - \frac{\Delta\lambda^n}{\Delta\eta_j}\left(\mathbf{G}^{n+1/2}_{i,j+1/2,k} - \mathbf{G}^{n+1/2}_{i,j-1/2,k}\right)\\ &- \frac{\Delta\lambda^n}{\Delta\zeta_k}\left(\mathbf{H}^{n+1/2}_{i,j,k+1/2} - \mathbf{H}^{n+1/2}_{i,j,k-1/2}\right).\end{aligned} \tag{55}$$

Step 4 (Decoding to get $\mathbf{U}_{i,j,k}^{n+1}$). This step is trivial; after it we have updated physical variables $\mathbf{Q}_{i,j,k}^{n+1}$ as well as geometrical variables $\mathbf{K}_{i,j,k}^{n+1}$.

Step 5 (Updating $h_{i,j,k}^{n}$ to $h_{i,j,k}^{n+1}$). This step is accomplished by solving Eq. (26), using the updated values $\mathbf{Q}_{i,j,k}^{n+1}$ and $\mathbf{K}_{i,j,k}^{n+1}$ in its coefficients. (Note: this step is, of course, to be bypassed if $h = \text{const.}$ is assumed in the computation).

Step 6 (Computation of the grid in the x–y–z space at λ^{n+1}). To calculate the grid at the next time step, trapezoidal integration is applied to get

$$\begin{cases} x_{i,j,k}^{n+1} = x_{i,j,k}^{n} + \frac{1}{2}\left(h_{i,j,k}^{n} u_{i,j,k}^{n} + h_{i,j,k}^{n+1} u_{i,j,k}^{n+1}\right)(\lambda^{n+1} - \lambda^{n}) \\ y_{i,j,k}^{n+1} = y_{i,j,k}^{n} + \frac{1}{2}\left(h_{i,j,k}^{n} v_{i,j,k}^{n} + h_{i,j,k}^{n+1} v_{i,j,k}^{n+1}\right)(\lambda^{n+1} - \lambda^{n}) \\ z_{i,j,k}^{n+1} = z_{i,j,k}^{n} + \frac{1}{2}\left(h_{i,j,k}^{n} w_{i,j,k}^{n} + h_{i,j,k}^{n+1} w_{i,j,k}^{n+1}\right)(\lambda^{n+1} - \lambda^{n}). \end{cases} \tag{56}$$

By a grid we mean the lines joining the cell centers, not the cell interface lines. We remark that the grid in the physical plane is not used in the computation (only the values of $\mathbf{K}$ are used) as the whole computation is carried out in the transformed space (the ξ–η–ζ space). So, this step is optional. However, the grid information is needed in computing steady flow as an asymptotic state of unsteady flow for large λ. In this case to check if a steady state is reached, which means the flow at every fixed location in the x–y–z plane does not change with increasing time, we should compare the flow variables $\mathbf{Q}$ at the same fixed points (x, y, z) in the physical space and not at the same fixed points (ξ, η, ζ) in the transformed plane; the latter are simply the pseudo-particles whose positions in the x–y–z space in general move with λ and never reach an asymptotic state.

After this, we repeat steps 2–6 to advance the solution further to λ^{n+2}, and so on.

6. TEST EXAMPLES

EXAMPLE 1. The first example is a pseudo three-dimensional Riemann problem. Two uniform flows with states

$$\mathbf{Q}_1 = (p, \rho, u, v, w) = (0.25, 0.5, 5.8566, 0, 0) \tag{57}$$

$$\mathbf{Q}_2 = (p, \rho, u, v, w) = (1.0, 1.0, 2.84, 0, 0.5) \tag{58}$$

as depicted in Fig. 1 are separated by the separating plane and begin to interact with each other at the intersection line. Theoretically, this class of problems was analyzed by Loh and Liou in [5]. In the computation, the steady flow is achieved with time marching until the flow structure and the variables do not change with time. A grid of $60 \times 100 \times 10$ with $\triangle\xi = \triangle\eta = \triangle\zeta = 0.01$ is employed in the computation. Initially, a grid with $\triangle x = \triangle y = \triangle z = 0.01$ in the physical plane is laid over a domain of $0 \le x \le 0.6$; $0 \le y \le 1.0$; $0 \le z \le 0.1$. The initial data are given at each cell according to its position in $y > 0.5$ or $y < 0.5$, representing cell-average values. The physical domain will change with time according to the pseudo-particle's velocity $h\mathbf{q}$ if h is not zero. If we follow the computational cells (pseudo-particles), they will move out of initial physical domain in x-direction as well as in z-direction, and it would be difficult to have a steady state of flow in the original physical domain. To avoid this, as it was done in 2-D computations ([1]), the "motionless viewing window" is applied in the x-direction.

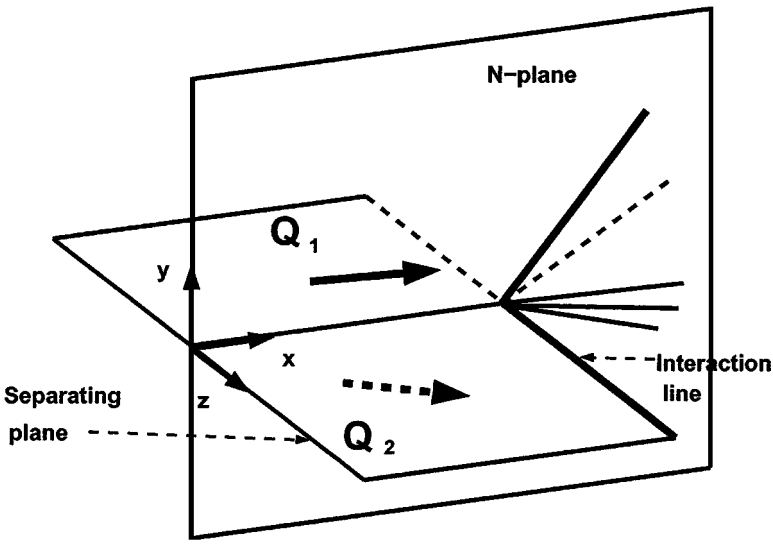

FIG. 1. Sketch of a steady pseudo 3-D Riemann problem.

In Figs. 2 and 4 are shown computed density using our unified code for $h = 0$ and $h = 0.999$. We can see that the result for $h = 0$ (Eulerian coordinates) is not satisfactory: slip line is poorly resolved and the computed density is far from an exact solution in the region between expansion fan and the slip line. This behavior of computed solution can be attributed to the fact that the slip line is always poorly resolved in Eulerian coordinates as a result of Godunov averaging across slip lines which, in general, do not coincide with coordinate lines. Moreover, the resolution of the slip line for the problem with

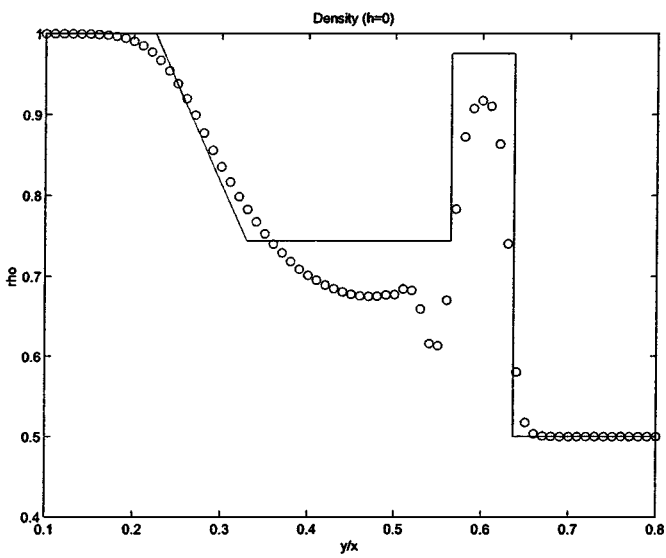

FIG. 2. Density distribution in the plane $z = \text{const.}$ in a steady pseudo 3-D Riemann problem computed by the present unified code, $h = 0$ (Eulerian).

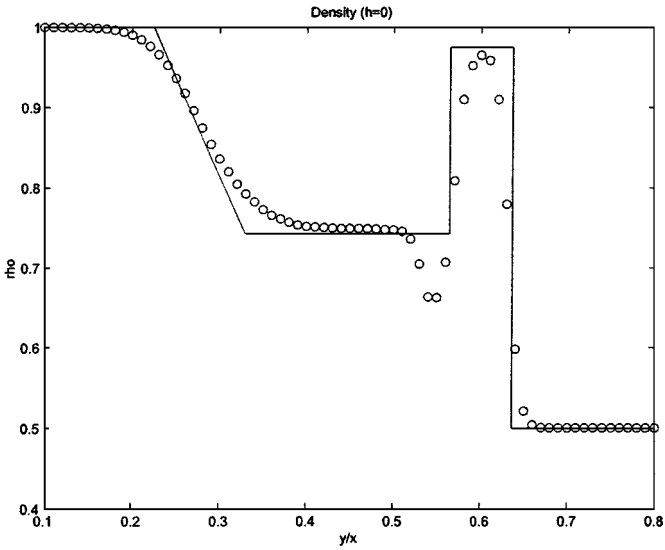

FIG. 3. Density distribution in the plane $z = \text{const.}$ in a steady 2-D Riemann problem computed by the present unified 3-D code, $h = 0$ (Eulerian).

initial conditions (58) is even worse than that in the test with purely two-dimensional initial conditions:

$$\mathbf{Q}_1 = (p, \rho, u, v, w) = (0.25, 0.5, 5.8566, 0, 0) \tag{59}$$

$$\mathbf{Q}_2 = (p, \rho, u, v, w) = (1.0, 1.0, 2.84, 0, 0.0). \tag{60}$$

This test for $h = 0$ with initial conditions (60) was computed using the 3-D code (Fig. 3), showing a very similar result to the result in [1, Fig. 5a], as expected.

A comparison of Figs. 2 and 4 shows that the slip line resolution greatly improves for $h = 0.999$ over $h = 0$, as expected. This is because the flow is steady and the slip surfaces coincide with the streamsurfaces which, in turn, coincide with the grid surfaces for $h = 0.999$, thus avoiding the Godunov averaging across slip surfaces.

Figure 5 shows the computed density using grid skewness preserving h as determined by Eq. (32), which is solved at each time step. As predicted, the slip line resolution is just as sharp as in the Lagrangian case ($h = 0.999$).

All the computations started with the Eulerian grid. The flow-generated grids, i.e., the lines joining the cell centers, at steady state are shown in Fig. 6 on the planes $\zeta = \text{const.}$ We note that (a) the grid for $h = 0.999$ is severely deformed near the slip line, and such grid deformation can cause inaccuracy locally [1]; (b) the grid using skewness preserving h is much more uniform everywhere although, unlike the 2-D case, is not orthogonal.

EXAMPLE 2. In the second example, we consider a truly three-dimensional, initial-boundary value problem—the supersonic inviscid corner flow. This problem was computed in [5] using a steady code which is valid only for purely supersonic flow. The geometrical configuration is shown in Fig. 7 ([6]). Two intersecting wedges, both with angle of 9.5°,

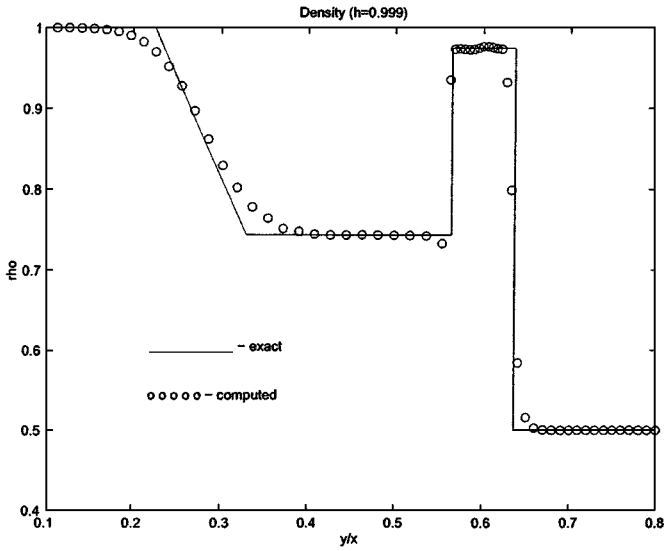

FIG. 4. Density distribution in the plane $\zeta = \text{const.}$ in a steady pseudo 3-D Riemann problem computed by the present unified code, $h = 0.999$ (Lagrangian).

form an axial corner over which there is a Mach 3 flow. The flow field consists of two planar wedge shocks, two embedded shocks, a corner shock, and the shear layers (slip surfaces) as shown in Fig. 8. We employ a mesh of $55 \times 45 \times 45$ in the x–y–z-space. This test was computed for $h = 0$ (Eulerian), $h = 0.999$, and for h chosen to preserve grid skewness. The contour plots are presented in the Figs. 9–11. The qualitative behavior of the computed

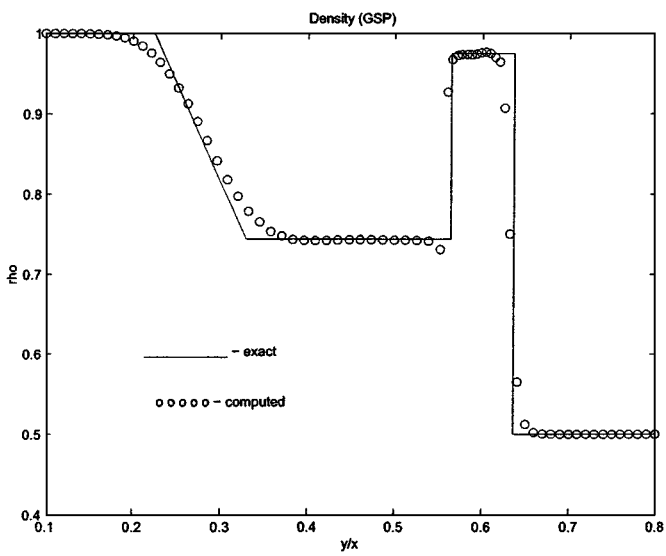

FIG. 5. Density distribution in the plane $\zeta = \text{const.}$ in a steady pseudo 3-D Riemann problem computed by the present unified code with h chosen to preserve grid skewness.

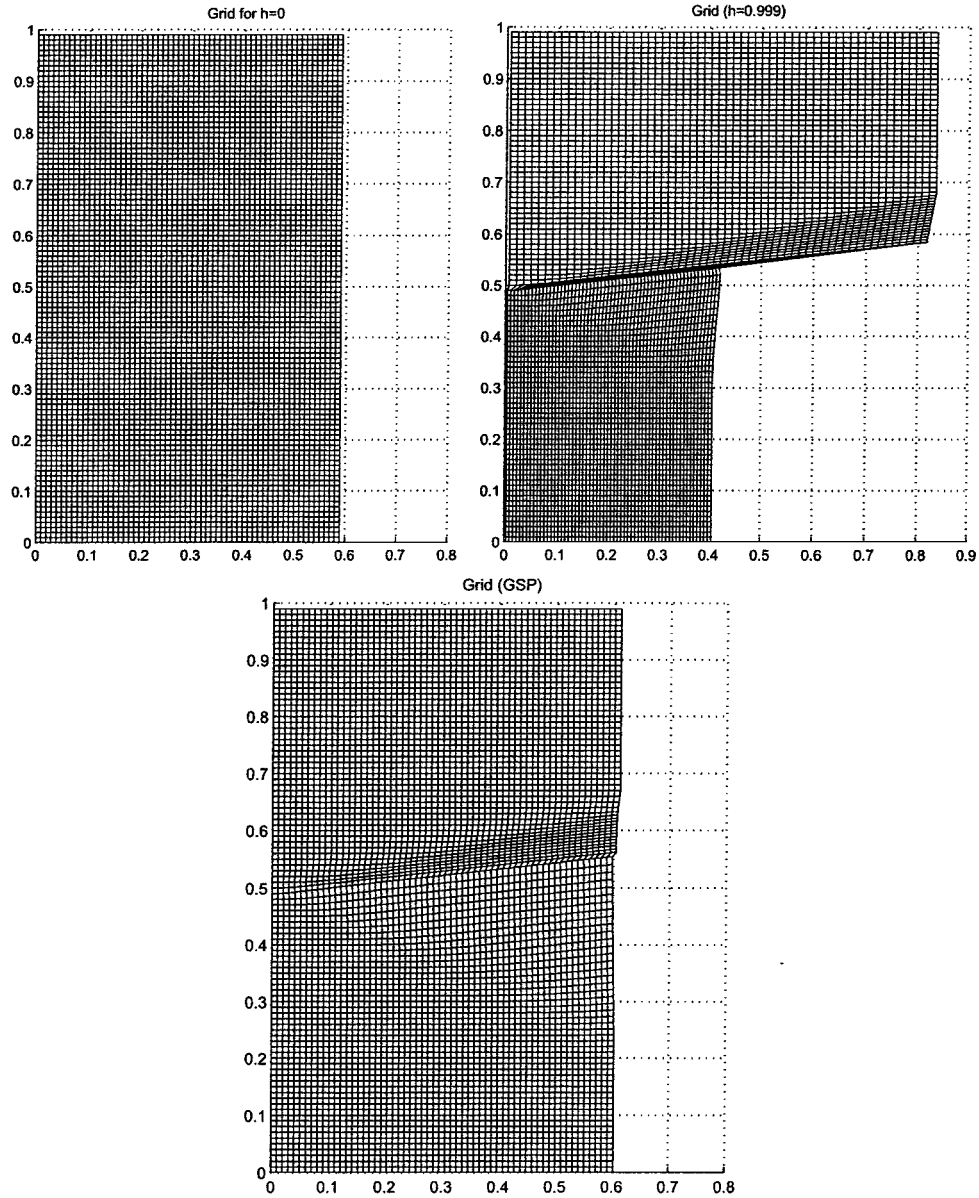

FIG. 6. Flow generated grids in the plane $\zeta = \text{const.}$ in the steady pseudo 3-D Riemann problem for: $h = 0$ (Eulerian) (top, left); $h = 0.999$ (Lagrangian) (top, right); h chosen to preserve grid skewness (bottom).

solutions is very similar to that presented in Fig. 8. The resolutions of slip surfaces in the case of grid skewness preserving h (Fig. 9) and in the Lagrangian case ($h = 0.999$) (Fig. 10) are similar and are clearly better than that for the Eulerian in Fig. 11. The experimental results from [6] are presented in the Fig. 12. The angle between the shear layers for grid skewness preserving h and for the Lagrangian case ($h = 0.999$) matches very well with the experimental result. With the corner shock aligned, the agreement for shocks between the experimental results (Fig. 12) and the Lagrangian results (Fig. 10) are also perfect: the

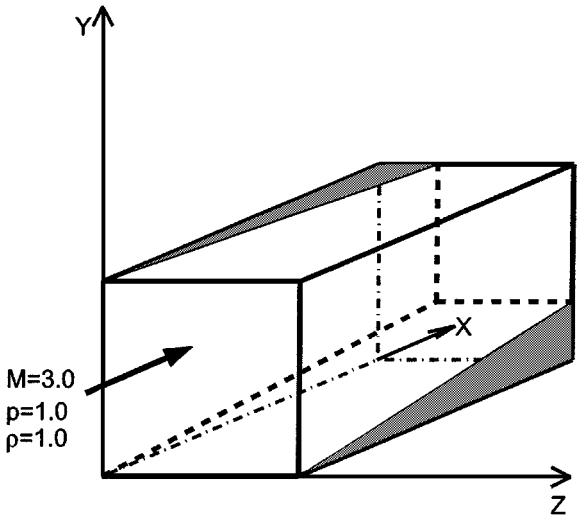

FIG. 7. Supersonic flow past a corner: sketch of the problem.

embedded shocks are curved which is in agreement with experiment. It can be explained by the fact that the pseudo-particles, which in the Lagrangian case are fluid particles, tend to crowd together when compressed, resulting in automatic refinement of the grid near shocks. Consequently, shock resolution is improved.

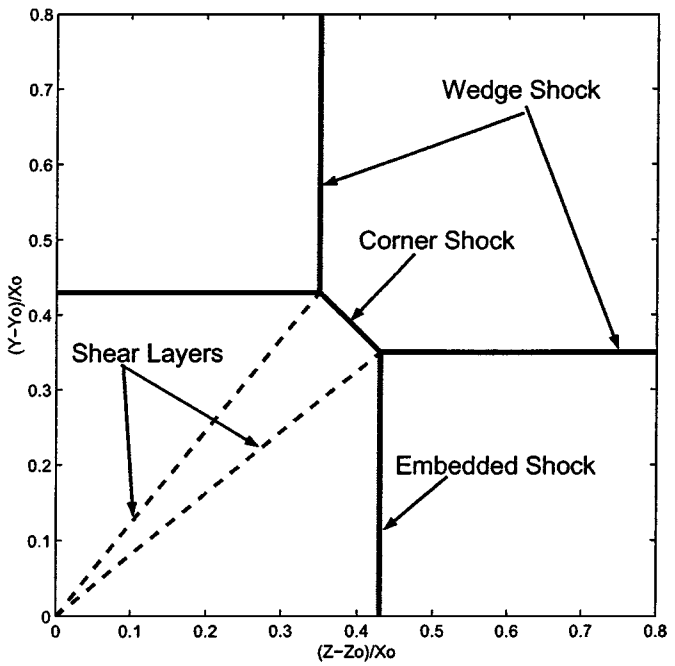

FIG. 8. Supersonic flow past a corner: structure of the flow [6].

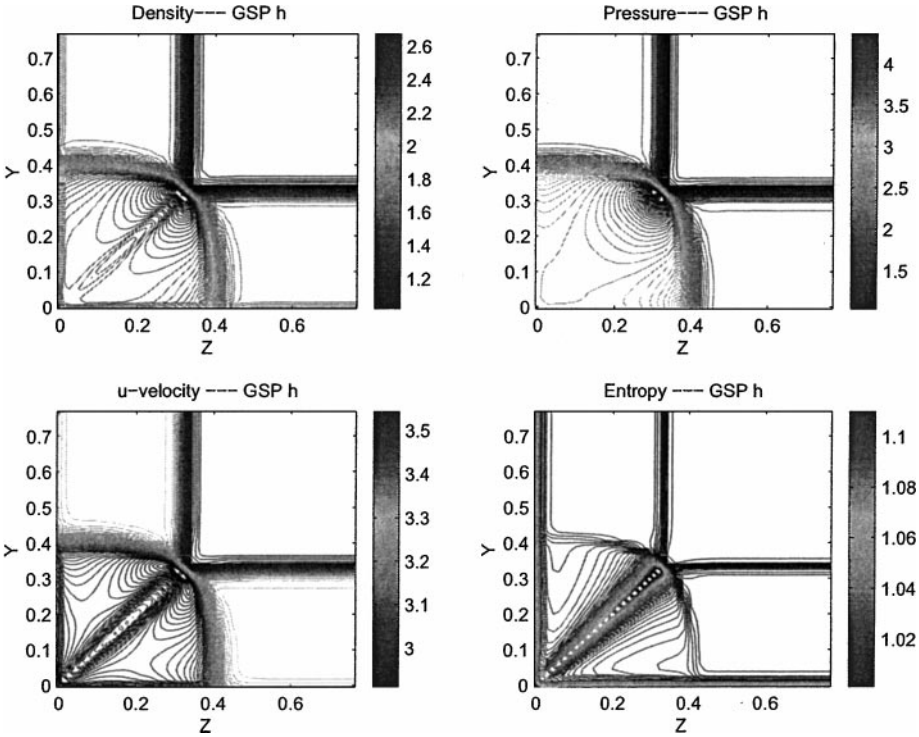

FIG. 9. Supersonic flow past a corner: contours of flow variables in the coordinates $Z = (z - z_0)/x_0$, $Y = (y - y_0)/x_0$, h chosen to preserve grid skewness.

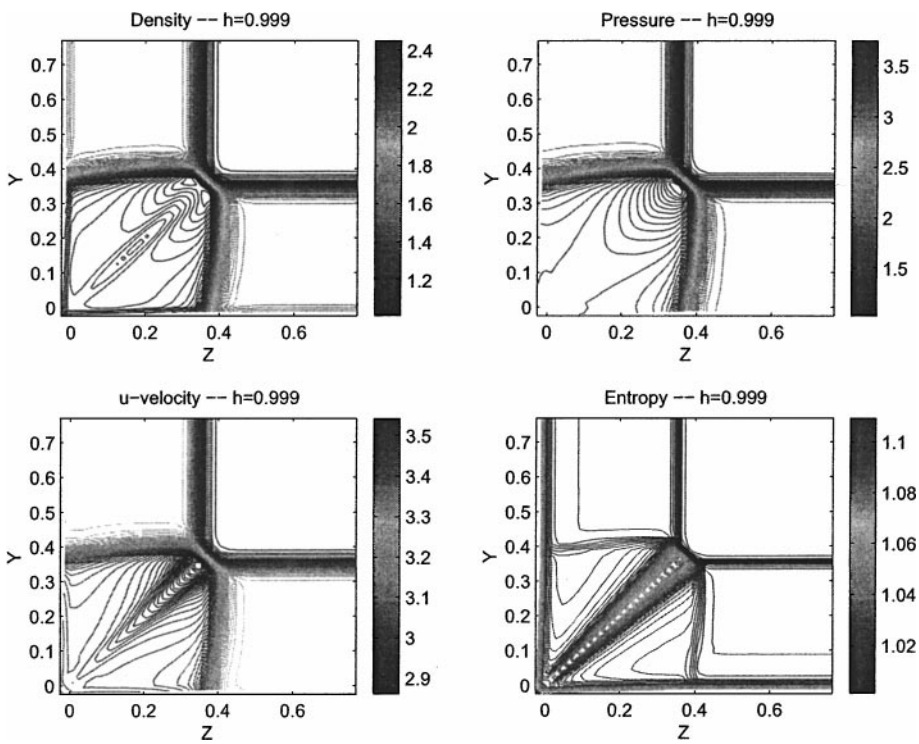

FIG. 10. Supersonic flow past a corner: contours of flow variables in the coordinates $Z = (z - z_0)/x_0$, $Y = (y - y_0)/x_0$, $h = 0.999$ (Lagrangian).

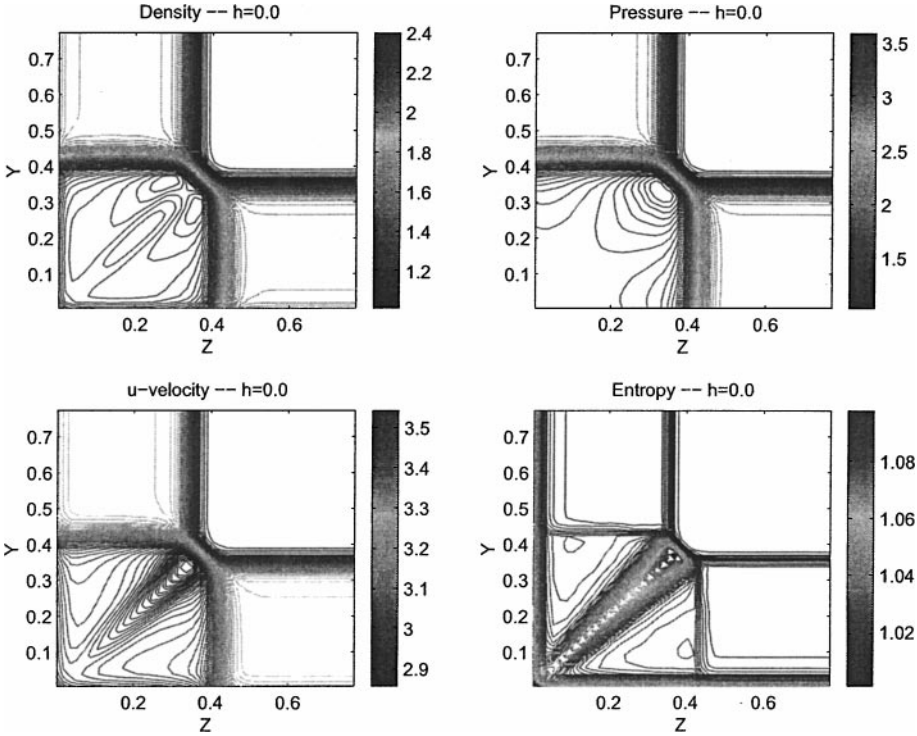

FIG. 11. Supersonic flow past a corner: contours of flow variables in the coordinates $Z = (z - z_0)/x_0$, $Y = (y - y_0)/x_0$, $h = 0$ (Eulerian).

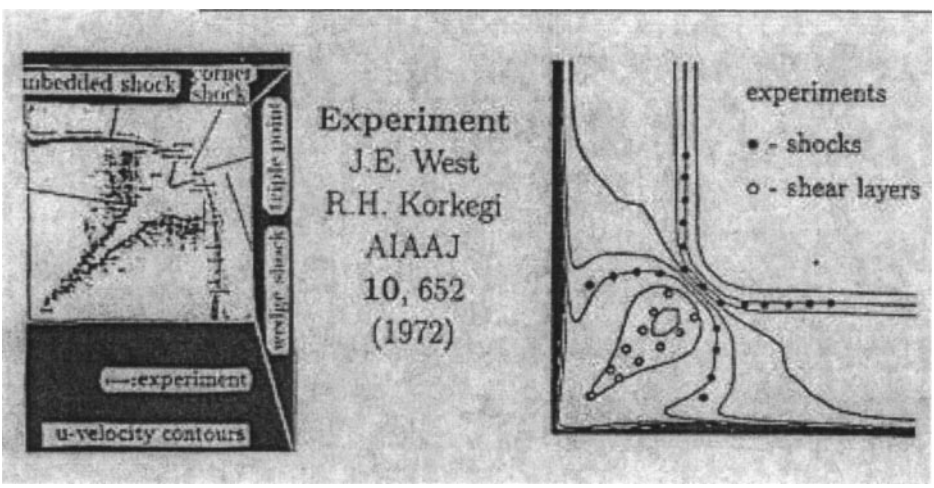

FIG. 12. Supersonic flow past a corner: experimental results reprinted from [6].

7. CONCLUSIONS

In this paper we have successfully extended the unified approach of Hui *et al*. [1] to the three-dimensional Euler equations of gas dynamics by choosing the free function h to preserve grid skewness. It has been tested on two problems and found that with the free function h so chosen, the unified coordinate system is superior to both Eulerian and Lagrangian system in that: (a) it resolves slip lines as sharply as the Lagrangian system, especially for steady flows, (b) it avoids the severe grid deformation of the Lagrangian system which causes inaccuracy and breakdown of computation.

APPENDIX A: SOLUTION TO THE RIEMANN PROBLEM (51)

We shall first find all possible solutions to (51) for $\xi > 0$ and $\xi < 0$ separately, and then use them to construct solution to the Riemann problem (51) for $-\infty < \xi < +\infty$.

Case 1. $\xi > 0$.

The Riemann problem is

$$\begin{cases} \frac{\partial \mathbf{E}}{\partial \lambda} + \frac{\partial \mathbf{F}}{\partial \xi} = 0 & \lambda > 0, \quad \xi > 0 \\ \mathbf{E}(0, \xi) = \mathbf{E}_r & \xi > 0, \end{cases} \tag{A.1}$$

where

$$\mathbf{E} = \begin{bmatrix} \rho\triangle \\ \rho\triangle\omega \\ \rho\triangle\tau_1 \\ \rho\triangle\tau_2 \\ \rho\triangle e \\ A \\ B \\ C \end{bmatrix}, \quad \mathbf{F} = S \begin{bmatrix} \rho(1-h)\omega \\ \rho(1-h)\omega^2 + p \\ \rho(1-h)\omega\tau_1 \\ \rho(1-h)\omega\tau_2 \\ \rho(1-h)\omega e + \omega p \\ -hu/S \\ -hv/S \\ -hw/S \end{bmatrix}$$

with $h = h_r = \text{const}$. Similarity solution to (A.1) exists in the form

$$\mathbf{E} = \mathbf{E}(\mu), \quad \mu = \frac{\xi}{\lambda}. \tag{A.2}$$

After rewriting the system (A.1) in a matrix form we can get the set of eigenvalues.

$$\sigma_1 = 0 \quad \text{(multiplicity of 3)} \tag{A.3}$$

$$\sigma_2 = \frac{S}{\triangle}(1-h)\omega \quad \text{(multiplicity of 3)} \tag{A.4}$$

$$\sigma_\pm = \frac{S}{\triangle}\{(1-h)\omega \pm a\}. \tag{A.5}$$

The corresponding set of right eigenvectors is

$$\mathbf{r}_1 = (0, 0, 0, 0, 0, 1, 0, 0)^T \tag{A.6}$$

$$\mathbf{r}_2 = (0, 0, 0, 0, 0, 0, 1, 0)^T \tag{A.7}$$

$$\mathbf{r}_3 = (0, 0, 0, 0, 0, 0, 0, 1)^T \tag{A.8}$$

$$\mathbf{r}_4 = (1, 0, 0, 0, 0, 0, 0, 0)^T \tag{A.9}$$

$$\mathbf{r}_5 = \left(0, 0, 0, 1, 0, \frac{h}{\sigma_2}\begin{vmatrix} i_2 & i_3 \\ k_2 & k_3 \end{vmatrix}, -\frac{h}{\sigma_2}\begin{vmatrix} i_1 & i_3 \\ k_1 & k_3 \end{vmatrix}, \frac{h}{\sigma_2}\begin{vmatrix} i_1 & i_2 \\ k_1 & k_2 \end{vmatrix}\right)^T \tag{A.10}$$

$$\mathbf{r}_6 = \left(0, 0, 0, 0, 1, -\frac{h}{\sigma_2}\begin{vmatrix} i_2 & i_3 \\ j_2 & j_3 \end{vmatrix}, \frac{h}{\sigma_2}\begin{vmatrix} i_1 & i_3 \\ j_1 & j_3 \end{vmatrix}, -\frac{h}{\sigma_2}\begin{vmatrix} i_1 & i_2 \\ j_1 & j_2 \end{vmatrix}\right)^T \tag{A.11}$$

$$\mathbf{r}_\pm = \left(a^{-2}, 1, \frac{\pm 1}{\rho a}, 0, 0, \frac{\mp h}{\rho a \sigma_\pm}\begin{vmatrix} j_2 & j_3 \\ k_2 & k_3 \end{vmatrix}, \frac{\pm h}{\rho a \sigma_\pm}\begin{vmatrix} j_1 & j_3 \\ k_1 & k_3 \end{vmatrix}, \frac{\mp h}{\rho a \sigma_\pm}\begin{vmatrix} j_1 & j_2 \\ k_1 & k_2 \end{vmatrix}\right)^T. \tag{A.12}$$

We shall now give solutions to the elementary waves in detail: the expansion wave, the shock wave, and the slip line. These solutions will be used in constructing the ξ-split Riemann solution to (51).

Smooth solutions. The expansion wave is a smooth solution corresponding to the $\sigma_\pm$ characteristic fields which can be derived from the following system of ODEs.

$$\frac{d\rho}{dp} = \frac{1}{a^2} \tag{A.13}$$

$$\frac{d\omega}{dp} = \pm\frac{1}{a\rho} \tag{A.14}$$

$$\frac{d\tau_1}{dp} = 0 \tag{A.15}$$

$$\frac{d\tau_2}{dp} = 0 \tag{A.16}$$

$$\frac{dA}{dp} = \mp\frac{h}{\rho a \sigma_\pm}\begin{vmatrix} j_2 & j_3 \\ k_2 & k_3 \end{vmatrix} \tag{A.17}$$

$$\frac{dB}{dp} = \pm\frac{h}{\rho a \sigma_\pm}\begin{vmatrix} j_1 & j_3 \\ k_1 & k_3 \end{vmatrix} \tag{A.18}$$

$$\frac{dC}{dp} = \mp\frac{h}{\rho a \sigma_\pm}\begin{vmatrix} j_1 & j_2 \\ k_1 & k_2 \end{vmatrix}. \tag{A.19}$$

The solutions for $\rho, \omega, \tau_1, \tau_2$ relate the flow state $\mathbf{Q} = (\rho, p, \omega, \tau_1, \tau_2)^T$ in the expansion fan to the initial state $\mathbf{Q}_0 = (\rho_0, p_0, \omega_0, (\tau_1)_0, (\tau_2)_0)^T$ upstream of the fan through the following expressions

$$\rho = \rho_0 \left(\frac{p}{p_0}\right)^{1/\gamma} \tag{A.20}$$

$$\omega = \omega_0 \pm \frac{2a_0}{\gamma - 1}\left(\left(\frac{p}{p_0}\right)^{\frac{\gamma-1}{2\gamma}} - 1\right) \tag{A.21}$$

$$\tau_1 = (\tau_1)_0 \tag{A.22}$$

$$\tau_2 = (\tau_2)_0, \tag{A.23}$$

where $a = (\frac{\gamma p}{\rho})^{1/2}$.

We remark that on crossing the expansion fan, these relations are independent of $\mathbf{K}_r$ and h_r.

To find the solution inside the expansion fan, we consider the characteristic ray through the origin $(0, 0)$ and a general point (λ, ξ) inside the fan. The slope of the characteristic ray is

$$\frac{d\xi}{d\lambda} = \frac{\xi}{\lambda} = \sigma_\pm = \frac{S}{\triangle}\{(1-h)\omega \pm a\}. \tag{A.24}$$

Using the above expression and the equation for ω in (A.21), we get

$$p = p_0 \left[\frac{2(1-h)}{\gamma - 2h + 1} \mp \frac{\gamma - 1}{(\gamma - 2h + 1)a_0}\left((1-h)\omega_0 - \frac{\triangle}{S}\mu\right)\right]^{(2\gamma/\gamma-1)}, \tag{A.25}$$

where $\triangle$ is found from (A.17)–(A.19) to be a function of p

$$\triangle = \triangle_0 e^{g(p)}, \quad g(p) = \mp \int_{p_0}^{p} \frac{h dp}{A_\pm p^{\frac{\gamma+1}{2\gamma}} + B_\pm p} \tag{A.26}$$

with

$$A_\pm = (1-h)\left(\omega_0 \mp \frac{2a_0}{\gamma - 1}\right)\rho_0 a_0 p_0^{-\frac{\gamma+1}{2\gamma}}$$

$$B_\pm = \frac{2\gamma(1-h)}{\gamma - 1} \pm \gamma.$$

Equations (A.25)–(A.26) define an implict function $p(\mu)$, $\mu = \frac{\xi}{\lambda}$. The expression for ρ, ω, τ_1, and τ_2 in terms of μ can be easily obtained from (A.20)–(A.23). Like p, they depend on $(\mathbf{K}_r, h_r)$, but at $\mu = 0$ they depend only on h_r. The variations of A, B, and C across an expansion fan can also be obtained from (A.17)–(A.19), but they are not needed in calculating the flux $\mathbf{F}$ and are thus not given here.

Discontinuous solutions. The Rankine–Hugoniot jump conditions of the system (A.1) are

$$s[\rho\triangle] = [\rho(1-h)\omega S] \tag{A.27}$$

$$s[\rho\triangle\omega] = [(\rho(1-h)\omega^2 + p)S] \tag{A.28}$$

$$s[\rho\triangle\tau_1] = [\rho(1-h)\omega\tau_1 S] \tag{A.29}$$

$$s[\rho\triangle\tau_2] = [\rho(1-h)\omega\tau_2 S] \tag{A.30}$$

$$s[\rho\triangle e] = [(\rho(1-h)\omega e + \omega p)S] \tag{A.31}$$

$$s[A] = -[hu] \tag{A.32}$$

$$s[B] = -[hv] \tag{A.33}$$

$$s[C] = -[hw], \tag{A.34}$$

where $[\cdot]$ denotes the jump across the discontinuity whose slope is denoted by $s = \frac{d\xi}{d\lambda}$.

Shock waves. The shock jump relations after some algebraic manipulations can be expressed in terms of $\alpha = \frac{p}{p_0}$ as follows:

$$s = \frac{S}{\triangle_0}\left[(1-h)\omega_0 \pm a_0\left(\frac{\gamma+1}{2\gamma}(\alpha-1)+1\right)^{1/2}\right] \tag{A.35}$$

$$\rho = \rho_0 \frac{\alpha(\gamma+1)+\gamma-1}{\alpha(\gamma-1)+\gamma+1} \tag{A.36}$$

$$\omega = \omega_0 \pm \frac{(\alpha-1)a_0}{(0.5\gamma[(\gamma+1)\alpha+\gamma-1])^{1/2}} \tag{A.37}$$

$$\tau_1 = (\tau_1)_0 \tag{A.38}$$

$$\tau_2 = (\tau_2)_0. \tag{A.39}$$

We remark that the relations of the flow variables (p, ρ, ω, τ) across the shock are independent of $\mathbf{K}_r$ and h_r, while the slope of the shock wave s is dependent on $\mathbf{K}_r$ and h_r. But this dependence is not needed in finding the pressure p, and hence also $(\rho, \omega, \tau_1, \tau_2)$, at $\mu = 0$ provided only that $s > 0$. (If $s < 0$, the shock wave will appear in the quadrant $(\xi < 0, \lambda > 0)$).

We note that the jumps of A, B, and C across a shock may also be obtained from (A.32)–(A.34), but they are not used in calculating the flux $\mathbf{F}$ and are thus not given here.

Slip lines. For the slip line corresponding to the speed $s = \sigma_2 = \frac{S}{\triangle_0}(1-h)\omega_0 > 0$ we find, from Rankine–Hugoniot jump conditions (A.27)–(A.34), that

$$p = p_0 \tag{A.40}$$

$$\omega = \omega_0 \tag{A.41}$$

but ρ, τ_1, τ_2 and A, B, C may jump arbitrarily.

We again remark that, except the speed s, the relations (A.40)–(A.41) across a slip line are independent of $(\mathbf{K}_r, h_r)$. Although s depends on $(\mathbf{K}_r, h_r)$, the dependence is not needed in calculating $(p, \rho, \omega, \tau_1, \tau_2)$ and the flux $\mathbf{F}$, provided $s > 0$. (If $s < 0$, the slip line appears in the quadrant $(\xi < 0, \lambda > 0)$.)

Case (2). $\xi < 0$.

The solution for $\xi < 0$ can be obtained similarly.

Now, after obtaining all possible solutions for $\xi > 0$ and $\xi < 0$ separately, the question is how to construct the solution to the Riemann problem for $\lambda > 0$, $-\infty < \xi < +\infty$. We find that at $\xi = 0$ the coefficients in $\mathbf{E}$ and $\mathbf{F}$ jump discontinuously. This is the difficulty one would face with in the Eulerian system using curvilinear coordinates rather than Cartesian coordinates.

The Riemann solution in the neighborhood of $\xi = 0$ is given by the σ_1-field whose speed is $s = 0$. The flow states on the two sides of cell interface $\xi = 0$ are related by (A.27)–(A.34) with $s = 0$. These are eight equations relating five jumps of p, ρ, ω, τ_1, and τ_2 and, therefore, in general have no solution, except when $h_r = h_l$, $L_r = L_l$, $M_r = M_l$, $N_r = N_l$, $P_r = P_l$, $Q_r = Q_l$, and $R_r = R_l$. In the latter case, there is a solution: the trivial solution $[p] = [\rho] = [\omega] = [\tau_1] = [\tau_2] = 0$, i.e., a continuous solution.

To avoid the difficulty of the non-existence of the solution to the Rankine–Hugoniot relations (A.27)–(A.34), we replace both h_l and h_r by their average, i.e., $h_l = h_r = 0.5(h_l + h_r) = \bar{h}$, and similarly replace L_l and L_r, M_l and M_r, N_l and N_r, P_l and P_r, Q_l and Q_r and R_l and R_r, by their averages $\bar{L}$, $\bar{M}$, $\bar{N}$, $\bar{P}$, $\bar{Q}$, and $\bar{R}$, respectively. Consequently, the Rankine–Hugoniot relations are satisfied and the flow is continuous across $\mu = \frac{\xi}{\lambda} = 0$. We note from previous discussions that these replacements do not alter the relations of the flow variables (ρ, p, ω, τ_1, τ_2) across the elementary waves (the expansion fan, the shock, and the slip line) as they do not depend on (**K**, h). It should be pointed out that the replacements of the geometric variables (L, M, N, P, Q, R) by their averages are a fictious one—they are invoked only to ensure the existence of solution to (A.27)–(A.34)—but these average values are never used in the computation. On the other hand, the replacement of h_l and h_r by $\bar{h}$ is a necessary one: it is used in Eq. (A.25) when the line $\mu = 0$ is inside the expansion fan.

The Riemann solution for $-\infty < \xi < +\infty$ can now be constructed in the usual way as if the slip line corresponding to $s = \sigma_1 = 0$ did not exist: shock (or expansion fan), slip line, and expansion fan (or shock), separated by uniform flow regions.

The η-split and ζ-split Riemann problems can be treated similarly.

ACKNOWLEDGMENTS

This research was funded by the Research Grants Council of Hong Kong to the senior author.

REFERENCES

1. W. H. Hui, P. Y. Li, and Z. W. Li, A unified coordinate system for solving the two-dimensional Euler equations, *J. Comput. Phys.* **153**, 596 (1999).
2. S. Kudriakov, *Unified Coordinates and Resolution of Discontinuities for Euler and Shallow Water Equations*, Ph.D. thesis (Hong Kong University of Science and Technology, 2000).
3. W. H. Hui and D. L. Chu, Optimal grid for the steady Euler equations, *Comput. Fluid Dyn. J.* **4**, 403 (1996).
4. W. H. Hui and Y. He, Hyperbolicity and optimal coordinates for the three-dimensional supersonic Euler equations, *SIAM J. Appl. Math.* **57**, No. 4, 893 (1997).
5. C. Y. Loh and M. S. Liou, A new Lagrangian method for three-dimensional steady supersonic flows, *J. Comput. Phys.* **113**, 224 (1994).
6. J. E. West and R. H. Korkegi, Supersonic interaction in the corner of intersecting wedges at high Reynolds numbers, *AIAA J.* **10**, 652 (1972).